High efficiency tomographic reconstruction of quantum states by quantum nondemolition measurements

J. S. Huang,[1] L. F. Wei*,[1,2] and C. H. Oh[†3]

[1]*Quantum Optoelectronics Laboratory, School of Physics and Technology,*
Southwest Jiaotong University, Chengdu 610031, China
[2]*State Key Laboratory of Optoelectronic Materials and Technologies,*
School of Physics and Engineering, Sun Yat-Sen University Guangzhou 510275, China
[3]*Centre for Quantum Technologies and Department of Physics,*
National University of Singapore, 3 Science Drive 2, Singapore 117542, Singapore

We propose a high efficiency tomographic scheme to reconstruct an unknown quantum state of the qubits by using a series of quantum nondemolition (QND) measurements. The proposed QND measurements of the qubits are implemented by probing the the stationary transmissions of the dispersively-coupled resonator. It is shown that only one kind of QND measurements is sufficient to determine all the diagonal elements of the density matrix of the detected quantum state. The remaining non-diagonal elements of the density matrix can be determined by other spectral measurements by beforehand transferring them to the diagonal locations using a series of unitary operations. Compared with the pervious tomographic reconstructions based on the usual destructively projective (DP) measurements (wherein one kind of such measurements could only determine one diagonal element of the density matrix), the present approach exhibits significantly high efficiency for N-qubit ($N > 1$). Specifically, our generic proposal is demonstrated by the experimental circuit-quantum-electrodynamics (circuit-QED) systems with a few Josephson charge qubits.

PACS number(s): 42.50.Pq, 03.65.Wj, 03.67.Lx, 85.25.Cp

I. INTRODUCTION

The reconstruction of an unknown quantum state from a suitable set of measurements is called quantum tomography [1], which is a particularly important method in the study of quantum mechanics and its various applications. Since the characterization of the states is the central tasks in quantum-state engineerings and controls, this technique is of great importance in the current quantum information processing. Recently, many theoretical analysis and experimental demonstrations have been devoted to implement the desirable quantum-state tomographies for, e.g., the polarization states of photons [2, 3], the electronic states of trapped ions [4], and the solid-state qubits [5], etc. However, all these tomographic reconstructions are based on the destructively-projective (DP) measurements, and thus are very operational-complicated. This is because that each kind of DP measurements, e.g., $\hat{P}_k = |k\rangle\langle k|$, is required to be performed many times on many copies of the reconstructed state for determining just one of the elements (e.g., $|c_k|^2$ in the state $|\psi\rangle = \sum_k c_k |k\rangle$) in the density matrix $\rho = |\psi\rangle\langle\psi|$.

Besides the usual DP measurements, quantum state could also be detected by other strategies, typically such as the so-called quantum nondemolition (QND) measurements. Basically, QND measurement is a nondestructive detection, as the measurement-induced back-action noises could be effectively suppressed by repeatedly hiding them in certain observables which are not of interests. The basic criteria for a QND measurement is that the repeated measurements of an observable $\hat{o}$ of the same system should yield the identical result. This means that the measured observable must be commutative with the Hamiltonian $\hat{H}_{int}$ describing the interaction between the measured system and the detector, i.e., $[\hat{H}_{int}, \hat{o}] = 0$. Historically, QND measurement is proposed to explore the fundamental limitations of measurements, and has been demonstrated in various branches of physics, such as in the detection of gravitational waves [6], quantum optics [7–9], telecommunications [10], and quantum control [11], etc. In recent years, the QND measurement has also been successfully applied to probe the atomic qubits in the cavity quantum electrodynamics (QED) [12, 13]. Furthermore, this technique was extensively used to the circuit QED systems [14–20] for nondestructively reading out the superconducting qubits. This QND measurement is implemented by measuring the transmission of the driven microwave signals through a transmission line resonator, which is dispersively coupled to the detected qubits. This is because that the detected qubits can cause sufficiently large state-dependent shifts of the resonator frequency. Thus by detecting the signals of the shifted frequency of the resonator, the qubit state will be read out. However, the QND measurements in the above works [14–20] are only utilized to effectively distinguish the different logic states of the detected qubit(s), which is (are) not prepared initially at their superposed state.

Motivated by the above experiments, recently we proposed a new scheme to nondestructively detect the superposition of these logic states by the QND measurements [21]. By taking account of the full quantum correlations between the resonator and dispersively-coupled qubit(s), our proposal shows that each detected peak marks one of the logic states and the relative height of such a peak is related to its corresponding superposed probability. This means that one kind of the QND measurements can determine all the diagonal elements of the density matrix of the measured quantum state $\rho = |\psi\rangle\langle\psi|$. Similarly, the non-diagonal elements of ρ could be determined

by other kinds of QND measurements by performing the suitable unitary operations to transfer them into the measurable diagonal locations. Therefore, the proposed tomographic reconstructing approach is high efficient for N ($N > 1$) qubits, as the number of the kinds of the QND measurements required is significantly decreased. For example, to tomographically reconstruct a two-qubit state, the proposed 6-kind QND measurements are sufficient. This is significantly simpler than the previous schemes (requiring 15-kind measurements) based on either the DPs [5] or the individual dispersive readouts of the logic states [20].

The paper is organized as follows: Sec. II gives our generic model of the transmissions of a driven resonator. In Sec. III, we provide a detailed analysis of the QND measurement of a single-qubit state by probing the transmissions of the driven resonator. Next, we show how to use these QND measurements to tomographically reconstruct an unknown single-qubit state in the experimental circuit-QED system. The extensions to the two-qubit case are given in Sec. IV, where the advantage of our proposal (compared with the previous approach based on the DP measurements) will be explicitly revealed. The possible generalization to the N-qubit situation and summarizations of our main results are finally given in Sec. V.

II. TRANSMISSION OF A DRIVEN EMPTY CAVITY

For the detection of the states of the qubits, we investigate the photon transmission of a driven resonator by studying the steady-state properties of the resonator-qubits dynamics. For generality, we consider a cavity-QED system consisting of N qubits. The Hamiltonian reads

$$H = \hbar\omega_r \hat{a}^\dagger \hat{a} + \sum_{j=1}^{N}[\frac{\hbar\omega_j}{2}\sigma_{z_j} + \hbar g_j(\sigma_{+_j}\hat{a} + \sigma_{-_j}\hat{a}^\dagger)], \quad (1)$$

where $a^{(\dagger)}$ and $\sigma_{\pm_j}$ are ladder operators for the photon field and the jth qubit respectively. Also, ω_r is the cavity frequency, ω_j the jth qubit transition frequency, and g_j the coupling strength between the jth qubit and the resonator. Suppose that the cavity is coherently driven by

$$H_d = \hbar\epsilon(\hat{a}^\dagger e^{-i\omega_d t} + \hat{a}e^{i\omega_d t}), \quad (2)$$

where ϵ is the real amplitude and ω_d the frequency of the applied external driving.

Under the Born-Markov approximation, the dynamics of the whole system with the dissipations and dephasings is described by the following master equation [22]

$$\dot{\varrho}_N = -\frac{i}{\hbar}[H_N, \varrho_N] + \kappa\mathcal{D}[a]\varrho_N + \sum_{j=1}^{N}\gamma_{1,j}\mathcal{D}[\sigma_{-_j}]\varrho_N$$

$$+ \sum_{j=1}^{N}\frac{\gamma_{\phi,j}}{2}\mathcal{D}[\sigma_{z_j}]\varrho_N, \quad (3)$$

$$H_N = H + H_d.$$

Here, ϱ_N is the density operator and the dissipation superoperator is defined by $\mathcal{D}[A]\varrho_N = A\varrho_N A^\dagger - A^\dagger A\varrho_N/2 - \varrho_N A^\dagger A/2$, which describes the effects of the environment on the system. The parameters of the last three terms in Eq. (3) correspond to photon decay rate κ, the jth qubit decay rate $\gamma_{1,j}$, and the jth qubit pure dephasing rate $\gamma_{\phi,j}$, respectively.

In what follows, we begin with the master equation (3) to calculate the frequency-dependent transmission of the cavity, which is proportional to the steady-state mean photon number $\langle\hat{a}^\dagger\hat{a}\rangle$ in the cavity. Technically, to satisfy the basic criteria for the desirable QND measurements of the N-qubit system, we assume that the conditions

$$0 < \frac{g_j}{\Delta_j}, \frac{g_j g_{j'}}{\Delta_j \Delta_{jj'}}, \frac{g_j g_{j'}}{\Delta_{j'}\Delta_{jj'}} \ll 1, \ j \neq j' = 1, 2, ..., N, \quad (4)$$

should be satisfied for assuring the effective dispersive coupling $\sigma_{z_j}\hat{a}^\dagger\hat{a}$ between the jth qubit and the cavity. These conditions assure also that the inter-bit interactions are negligible. Above, $\Delta_j = \omega_j - \omega_r$ denotes the detuning between the jth qubit and the cavity, and $\Delta_{jj'} = \omega_j - \omega'_j$ the detuning between the jth and j'th qubits.

For contrast, we first calculate the transmission spectrum of a driven empty cavity. The Hamiltonian of the simplified system reduces to ($\hbar = 1$ throughout the paper)

$$H_0 = \omega_r\hat{a}^\dagger\hat{a} + \epsilon(\hat{a}^\dagger e^{-i\omega_d t} + \hat{a}e^{i\omega_d t}). \quad (5)$$

After the time-dependent unitary transformation defined by the operator $R = \exp(-i\omega_d t\hat{a}^\dagger\hat{a})$, we get the effective Hamiltonian

$$\tilde{H}_0 = R^\dagger H_0 R - iR^\dagger\partial R/\partial t = -\Delta_{dr}\hat{a}^\dagger\hat{a} + \epsilon(\hat{a}^\dagger + \hat{a}), \quad (6)$$

where $\Delta_{dr} = \omega_d - \omega_r$ is the detuning of the cavity from the driving. Consequently, we get the master equation for such a driven empty cavity

$$\dot{\varrho}_0 = -i[\tilde{H}_0, \varrho_0] + \kappa(\hat{a}\varrho_0\hat{a}^\dagger - \hat{a}^\dagger\hat{a}\varrho_0/2 - \varrho_0\hat{a}^\dagger\hat{a}/2), (7)$$

where ϱ_0 is the density matrix of the empty cavity.

From the above master equation, one can easily obtain the equations of motion for the expectation values of the relevant operators, such as mean photon number inside the cavity $\langle\hat{a}^\dagger\hat{a}\rangle = Tr(\hat{a}^\dagger\hat{a}\varrho_0)$:

$$\frac{d\langle\hat{a}^\dagger\hat{a}\rangle}{dt} = -\kappa\langle\hat{a}^\dagger\hat{a}\rangle - 2\epsilon\text{Im}\langle\hat{a}\rangle, \quad (8a)$$

with

$$\frac{d\langle\hat{a}\rangle}{dt} = (i\Delta_{dr} - \frac{\kappa}{2})\langle\hat{a}\rangle - i\epsilon. \quad (8b)$$

The steady-state solution of Eq. (8) gives

$$\frac{\langle\hat{a}^\dagger\hat{a}\rangle_{ss}}{\epsilon^2} = \frac{1}{(\omega_d - \omega_r)^2 + (\frac{\kappa}{2})^2}. \quad (9)$$

Obviously, the transmission spectrum of an empty cavity, which is proportional to $\langle\hat{a}^\dagger\hat{a}\rangle$, is well-known Lorentzian: centered at $\omega_d = \omega_r$ with the half-width κ. Certainly, when ω_d does not sufficiently match the cavity frequency, no photon penetrates the cavity and thus no transmission is recorded.

III. TOMOGRAPHIC RECONSTRUCTION OF A SINGLE-QUBIT STATE BY QND MEASUREMENTS

A. Nondestructive detection of a single qubit by cavity transmissions

Now we investigate the case, in which a single qubit with transition frequency ω_1 is dispersively coupled to the cavity mode. In the frame rotating at drive frequency ω_d characterized by the transformation R, the Hamiltonian of the system reads

$$\tilde{H}_1 = \frac{\tilde{\omega}_1}{2}\sigma_{z_1} + (-\Delta_{dr} + \Gamma_1\sigma_{z_1})\hat{a}^\dagger\hat{a} + \epsilon(\hat{a}^\dagger + \hat{a}), \quad (10)$$

with $\tilde{\omega}_1 = \omega_1 + \Gamma_1$ and $\Gamma_1 = g_1^2/\Delta_1$.

Under the Born-Markov approximation, the master equation for the single-qubit plus the driven resonator is

$$\dot{\varrho}_1 = -i[\tilde{H}_1, \varrho_1] + \kappa\mathcal{D}[a]\varrho_1 + \gamma_{1,1}\mathcal{D}[\sigma_{-1}]\varrho_1 + \frac{\gamma_{\phi,1}}{2}\mathcal{D}[\sigma_{z_1}]\varrho_1. \quad (11)$$

The desirable quantity $\langle\hat{a}^\dagger\hat{a}\rangle$ can be determined by solving the following coupled equations of motion:

$$\frac{d\langle\hat{a}^\dagger\hat{a}\rangle}{dt} = -\kappa\langle\hat{a}^\dagger\hat{a}\rangle - 2\epsilon\mathrm{Im}\langle\hat{a}\rangle, \quad (12a)$$

$$\frac{d\langle\hat{a}\rangle}{dt} = (i\Delta_{dr} - \frac{\kappa}{2})\langle\hat{a}\rangle - i\Gamma_1\langle\hat{a}\sigma_{z_1}\rangle - i\epsilon, \quad (12b)$$

$$\frac{d\langle\hat{a}\sigma_{z_1}\rangle}{dt} = (i\Delta_{dr} - \frac{\kappa}{2} - \gamma_{1,1})\langle\hat{a}\sigma_{z_1}\rangle - (i\Gamma_1 + \gamma_{1,1})\langle\hat{a}\rangle - i\epsilon\langle\sigma_{z_1}\rangle, \quad (12c)$$

and

$$\frac{d\langle\sigma_{z_1}\rangle}{dt} = -\gamma_{1,1}(\langle\sigma_{z_1}\rangle + 1). \quad (12d)$$

It is obvious that the additional measurement-induced dephasing rate $\gamma_{\phi,1}$ does not influence the solution of the equations. As the decay $\gamma_{1,1}$ of the qubit is significantly less than the decay rate κ of the driven cavity, the average of σ_{z_1} could be safely assumed to be unchanged during the measurement. In fact, the characterized time of the detection is determined mainly by the decay of the cavity κ. Such a quantity is about $2\pi \times 1.69$ MHZ [19], which is obviously larger than $\gamma_{1,1} = 2\pi \times 0.02$ MHZ [16]. Experimentally, the time interval of completing a single QND measurement is about $T_e = 40$ns [19], this is significantly shorter than the lifetime: $T_1 \sim 7.3\mu$s and the decoherence time: $T_2 \sim 500$ns [16]. Therefore, during such a readout the decay of the qubit is negligible, i.e., $\langle\sigma_{z1}(T_e)\rangle = \exp(-\gamma_{1,1}T_e)(\langle\sigma_{z1}(0)\rangle + 1) - 1 \approx \langle\sigma_{z1}(0)\rangle$.

Under the steady-state condition, we obtain

$$\frac{\langle\hat{a}^\dagger\hat{a}\rangle_{ss}}{\epsilon^2}$$
$$= \frac{2}{\kappa} \times [(\frac{\kappa}{2} + \gamma_{1,1})(\frac{\kappa^2}{4} + \frac{\gamma_{1,1}\kappa}{2} + \Gamma_1^2 - \Delta_{dr}^2) + (\Delta_{dr} + \Gamma_1\langle\sigma_{z_1}(0)\rangle)(\kappa\Delta_{dr} + \gamma_{1,1}\Delta_{dr} + \gamma_{1,1}\Gamma_1)]$$
$$\times[(\frac{\kappa^2}{4} + \frac{\gamma_{1,1}\kappa}{2} + \Gamma_1^2 - \Delta_{dr}^2)^2 + (\kappa\Delta_{dr} + \gamma_{1,1}\Delta_{dr} + \gamma_{1,1}\Gamma_1)^2]^{-1}, \quad (13)$$

which is strongly related to the the initial state of qubit, thus the qubit state could be determined by the cavity transmission.
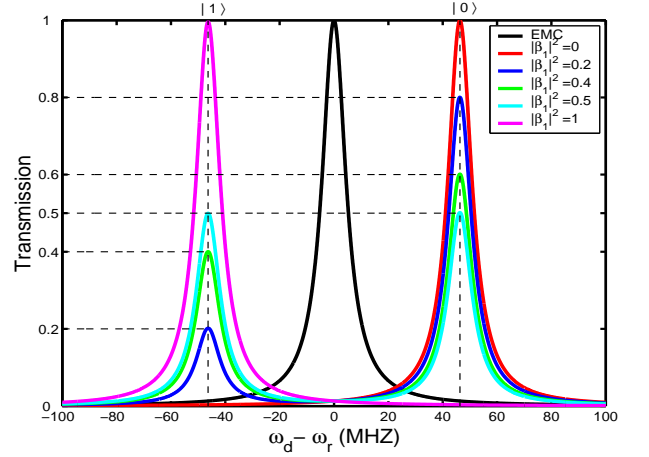

FIG. 1: (Color online) Cavity transmission for the single-qubit states versus the probe detuning $\omega_d - \omega_r$. Five cases of the qubit states for $|\beta_1|^2 = 0, 0.2, 0.4, 0.5,$ and 1 are shown. For comparison, the empty cavity (EMC) transmission is also plotted in black line. The peak shifts by $-\Gamma_1$ or Γ_1 correspond to single logic state $|0\rangle$ or $|1\rangle$. For the superposition states, the double-peak relative heights (in contrast to the peak height of the empty cavity transmission) present clearly the superposed probabilities of the two logic states. Here, the parameters are selected as: $(\Gamma_1, \kappa, \gamma_{1,1}) = 2\pi \times (-7.38, 1.69, 0.02)$MHz [16, 19].

The measured cavity transmission (normalized to the peak height of the empty cavity transmission) versus the probe frequency detuning are plotted in Fig. 1. Generally, the qubit is assumed to be prepared initially in the state $|\psi\rangle = \beta_0|0\rangle + \beta_1|1\rangle$. Obviously, when $\beta_0 = 0$, or 1, it reduces to the single logic state $|1\rangle$ or $|0\rangle$. Compared with the empty cavity transmission (plotted as the dark line in Fig. 1), one observes that qubit-resonator coupling leads to a right (left) shift of the single peak in the transmission spectrum by a quantity $-\Gamma (\Gamma)$, which is dependent of the logic states for $\langle\sigma_{z_1}(0)\rangle = -1 (\langle\sigma_{z_1}(0)\rangle = 1)$. Thus, the shifts of the peaks can be used to mark the logic states of the qubit. However, when the qubit is in the superposition of the two logic states, e.g., $|\beta_1|^2 = 0.2, 0.4,$ and 0.5, respectively, we see that the situation is very different from the case for the single logic states. In this case, the spectrum shows two peaks whose locations coincide with that for the single logic states, but the relative heights of these two peaks correspond clearly to the

superposed probabilities, i.e., $|\beta_0|^2$ and $|\beta_1|^2$, respectively. This provides an effective approach to directly measure the superposed probabilities of a superposed state.

B. Tomographic reconstruction of a single-qubit state

Above investigation indicates that, partial information of the qubit state, i.e., the diagonal elements of the relevant density matrix, can be directly obtained by only one kind of the QND measurements. While, to extract the full information of an unknown qubit state, one should tomographically reconstruct all the elements of its density matrix. Basically, to completely define a d-dimensional density matrix ρ, one needs to determine $d^2 - 1$ real parameters. Therefore, to determine an unknown qubit state, the key point is to identify these parameters by virtue of the tomographic technique.

Now we demonstrate how to perform the tomographic construction of an arbitrary single-qubit state $|\psi\rangle_1 = \beta_0|0\rangle + \beta_1|1\rangle$, whose density matrix operator reads

$$\rho_1 = \begin{pmatrix} \rho_{00} & \rho_{01} \\ \rho_{10} & \rho_{11} \end{pmatrix}. \tag{14}$$

A more efficient and widely used technique is to parameterize the density matrix ρ_1 on a Bloch sphere [5],

$$\rho_1 = \frac{1}{2}(I + \sum_{i=x,y,z} r_i \sigma_i) = \frac{1}{2}\begin{pmatrix} 1 + r_z & r_x - ir_y \\ r_x + ir_y & 1 - r_z \end{pmatrix}. \tag{15}$$

Here, I denotes the identity matrix, σ_i the Pauli matrices, and r_i real parameters. Therefore, in order to determine the single-qubit state, we must identify the three components (r_x, r_y, r_z) of the Bloch vector $\vec{r}$. As discussed in the previous section, two diagonal elements ρ_{00} and ρ_{11} of the density matrix ρ_1 can be directly determined by the two measured occupation probabilities $|\beta_0|^2$, $|\beta_1|^2$ in the direct QND measurements. This means that the parameter r_z can be determined by the relation $r_z = \rho_{00} - \rho_{11} = |\beta_0|^2 - |\beta_1|^2$. To obtain the other two parameters r_x and r_y, we need to determine the non-diagonal elements. To this end, we perform the single-qubit operations: $U_{x_1} = \exp(i\pi\sigma_{x_1}/4)$ and $U_{y_1} = \exp(i\pi\sigma_{y_1}/4)$, to transfer them to the the relevant diagonal locations, respectively. For example, after the operation U_{x_1}, the density matrix ρ_1 is changed to

$$\rho_1' = U_{x_1}\rho_1 U_{x_1}^\dagger = \frac{1}{2}\begin{pmatrix} 1 - r_y & r_x - ir_z \\ r_x + ir_z & 1 + r_y \end{pmatrix}. \tag{16}$$

Now, performing another kind of QND measurements the parameters $|\beta_0'|^2$ and $|\beta_1'|^2$ can be measured. Consequently, the coefficient r_y can be determined via the relation $r_y = |\beta_1'|^2 - |\beta_0'|^2$. Similarly, by performing the quantum operation U_{y_1} on the original density matrix ρ_1, another new density matrix

$$\rho_1'' = U_{y_1}\rho_1 U_{y_1}^\dagger = \frac{1}{2}\begin{pmatrix} 1 + r_x & -r_z - ir_y \\ -r_z + ir_y & 1 - r_x \end{pmatrix}, \tag{17}$$

can be obtained and the coefficient r_x can be similarly determined. Note that here the number of the unitary operations required for implementing the quantum state tomography (based on the QND measurements) is the same as the previous approach (based on the usual DP measurements). Thus, for the single-qubit case the complexity of the present approach is the same as that in the previous one. Note that here, as the same as that in the previous approach based on the DP measurements, three kinds of QND measurements are still required for the present reconstructions. One is directly applied, another is applied after the U_{x_1} operation, and the final one is applied after the U_{y_1} operation, thus the efficiency is not enhanced.

The remaining task is to implement the single-qubit operations required above for transferring the non-diagonal elements to the diagonal locations. We work with a circuit-QED system wherein a superconducting charge qubit is coupled to the fundamental mode of a transmission line resonator [23]. Let the qubit work at its degeneracy point and neglect the fast oscillating terms under the rotating-wave approximation (RWA). Following Ref. [24], under one displacement transformation, the effective Hamiltonian of the resonator plus qubit system can be written as

$$\tilde{H} = -\Delta_{dr}\hat{a}^\dagger\hat{a} + \frac{\Delta_a}{2}\sigma_{z_1} + g_1(\hat{a}^\dagger\sigma_{-_1} + \hat{a}\sigma_{+_1}) + \frac{\Omega}{2}\sigma_{x_1}, \tag{18}$$

with the detuning of the qubit transition frequency from the drive $\Delta_a = \omega_1 - \omega_d$ and the Rabi frequency $\Omega = 2\epsilon g_1/(-\Delta_{dr})$. Next, supposing that this system works in the dispersive regime, i.e., $|g_1/\Delta_1| \ll 1$, after the transformation $U_1 = \exp[-g_1(\hat{a}^\dagger\sigma_{-_1} - \hat{a}\sigma_{+_1})/\Delta_1]$, then the above Hamiltonian becomes

$$H_x = -\Delta_{dr}\hat{a}^\dagger\hat{a} + \frac{\tilde{\Delta}_a}{2}\sigma_{z_1} + \frac{\Omega}{2}\sigma_{x_1}, \quad \tilde{\Delta}_a = \Delta_a + \Gamma_1. \tag{19}$$

First, if the condition $\tilde{\Delta}_a = 0$ is satisfied, then the Hamiltonian (19) produces a rotation of the qubit about the x axis, i.e., U_{x_1} could be generated by choosing the evolution time $t_x = \pi/(2\Omega)$. Second, if the driving is sufficiently detuned from the qubit and its amplitude is also sufficiently large enough, then another approximate Hamiltonian

$$H_z = -\Delta_{dr}\hat{a}^\dagger\hat{a} + \frac{1}{2}(\tilde{\Delta}_a + \frac{1}{2}\frac{\Omega^2}{\Delta_a})\sigma_{z_1}, \tag{20}$$

can be obtained by further performing a transformations $U_2 = \exp(\beta^*\sigma_{+_1} - \beta\sigma_{-_1})$, with the coefficient $\beta = \Omega/(2\Delta_a)$, on the Hamiltonian (19). Obviously, the desirable operation U_{z_1} can be implemented by the evolution under the Hamiltonian (20) with the duration $t_z = \pi\Delta_a/(2\Delta_a\tilde{\Delta}_a + \Omega^2)$. Third, the desirable operation U_{y_1} could be constructed as: $U_{y_1} = \exp(i\pi\sigma_{y_1}/4) = \exp(i\pi\sigma_{z_1}/4)\exp(i3\pi\sigma_{x_1}/4)\exp(i3\pi\sigma_{z_1}/4)$. It should be pointed out that the durations t_x (or t_y) of the single-qubit operations required above for implementing the desirable tomographies is estimated as ~ 100ps using the experimental parameters: $\epsilon \sim 2\pi \times 20$MHz [18], and $\Delta_{dr} \sim \kappa/2$ [24]. This

is significantly less by at least two orders than the qubit decoherence time, which is measured as ~ 500ns [24]. Therefore, the required gate operations are accessible and the proposed tomographic reconstructions are experimentally feasible.

As an example, we assume that the three parameters $r_x = 0.6$, $r_y = 0.5$, $r_z = 0.6$ are obtained through the above reconstructions, then the reconstructed state ρ_1 can be written as $\rho_1 = 0.8|0\rangle\langle 0| + (0.3 - 0.25i)|0\rangle\langle 1| + (0.3 + 0.25i)|1\rangle\langle 0| + 0.2|1\rangle\langle 1|$, whose real $\rho_{ij}^{(R)}$ and imaginary $\rho_{ij}^{(I)}$ parts (i, j=0, 1) are graphically represented in Fig. 2.
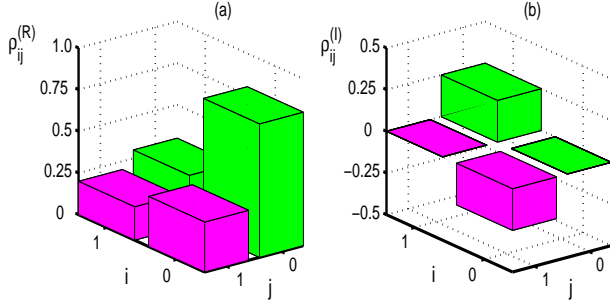

FIG. 2: (Color online) Graphic representations of the density matrix ρ_1 for a single-qubit state. The real $\rho_{ij}^{(R)}$ and imaginary $\rho_{ij}^{(I)}$ parts of the density matrix elements $\rho_{ij} = \langle i|\rho|j\rangle$ (i, j=0, 1) are plotted in (a) and (b), respectively.

IV. TOMOGRAPHIC RECONSTRUCTION OF A TWO-QUBIT STATE BY QND MEASUREMENTS

A. Nondestructive detection of an unknown two-qubit state by cavity transmissions

We extend the above sing-qubit QND measurements to the two-qubit case. The transition frequencies of the two qubits are represented as ω_1 and ω_2, respectively. In the above dispersive condition (4) and in a framework rotating at ω_d, the effective Hamiltonian of the present complete system is

$$\tilde{H}_2 = (-\Delta_{dr} + \Gamma_1\sigma_{z_1} + \Gamma_2\sigma_{z_2})\hat{a}^\dagger\hat{a} + \frac{\tilde{\omega}_1}{2}\sigma_{z_1} + \frac{\tilde{\omega}_2}{2}\sigma_{z_2} + \epsilon(\hat{a}^\dagger + \hat{a}), \quad (21)$$

where $\Gamma_j = g_j^2/\Delta_j$ and $\tilde{\omega}_j = \omega_j + \Gamma_j$, $j = 1, 2$.

Similarly, the relevant master equation reads

$$\dot{\varrho}_2 = -i[\tilde{H}_2, \varrho_2] + \kappa\mathcal{D}[a]\varrho_2 + \sum_{j=1,2} \gamma_{1,j}\mathcal{D}[\sigma_{-j}]\varrho_2 + \sum_{j=1,2} \frac{\gamma_{\phi,j}}{2}\mathcal{D}[\sigma_{z_j}]\varrho_2. \quad (22)$$

and the equations of motion for the mean values of various expectable operators are

$$\frac{d\langle\hat{a}^\dagger\hat{a}\rangle}{dt} = -\kappa\langle\hat{a}^\dagger\hat{a}\rangle - 2\epsilon\text{Im}\langle\hat{a}\rangle, \quad (23a)$$

$$\frac{d\langle\hat{a}\rangle}{dt} = (i\Delta_{dr} - \frac{\kappa}{2})\langle\hat{a}\rangle - i\Gamma_1\langle\hat{a}\sigma_{z_1}\rangle - i\Gamma_2\langle\hat{a}\sigma_{z_2}\rangle - i\epsilon, \quad (23b)$$

$$\frac{d\langle\hat{a}\sigma_{z_1}\rangle}{dt} = (i\Delta_{dr} - \frac{\kappa}{2} - \gamma_{1,1})\langle\hat{a}\sigma_{z_1}\rangle - (i\Gamma_1 + \gamma_{1,1})\langle\hat{a}\rangle - i\Gamma_2\langle\hat{a}\sigma_{z_1}\sigma_{z_2}\rangle - i\epsilon\langle\sigma_{z_1}\rangle, \quad (23c)$$

$$\frac{d\langle\hat{a}\sigma_{z_2}\rangle}{dt} = (i\Delta_{dr} - \frac{\kappa}{2} - \gamma_{1,2})\langle\hat{a}\sigma_{z_2}\rangle - (i\Gamma_2 + \gamma_{1,2})\langle\hat{a}\rangle - i\Gamma_1\langle\hat{a}\sigma_{z1}\sigma_{z_2}\rangle - i\epsilon\langle\sigma_{z_2}\rangle, \quad (23d)$$

$$\frac{d\langle\hat{a}\sigma_{z_1}\sigma_{z_2}\rangle}{dt} = (i\Delta_{dr} - \frac{\kappa}{2} - \gamma_{1,1} - \gamma_{1,2})\langle\hat{a}\sigma_{z_1}\sigma_{z_2}\rangle - i\epsilon\langle\sigma_{z_1}\sigma_{z_2}\rangle - (i\Gamma_2 + \gamma_{1,2})\langle\hat{a}\sigma_{z_1}\rangle - (i\Gamma_1 + \gamma_{1,1})\langle\hat{a}\sigma_{z_2}\rangle, \quad (23e)$$

$$\frac{d\langle\sigma_{z_1}\rangle}{dt} = -\gamma_{1,1}(\langle\sigma_{z_1}\rangle + 1), \quad (23f)$$

$$\frac{d\langle\sigma_{z_2}\rangle}{dt} = -\gamma_{1,2}(\langle\sigma_{z_2}\rangle + 1), \quad (23g)$$

$$\frac{d\langle\sigma_{z_1}\sigma_{z_2}\rangle}{dt} = -(\gamma_{1,1} + \gamma_{1,2})\langle\sigma_{z_1}\sigma_{z_2}\rangle - \gamma_{1,1}\langle\sigma_{z_2}\rangle - \gamma_{1,2}\langle\sigma_{z_1}\rangle. \quad (23h)$$

Again, due to the relatively-long decoherence times of the qubits and their sufficiently short measured times, the additional measurement-induced dephasing and decay rates of the qubits are also unimportant. Thus, the expectable values of the qubit operators can still be regarded as unchanged, i.e., $\langle\sigma_{z_j}(t)\rangle \approx \langle\sigma_{z_j}(0)\rangle$ and $\langle\sigma_{z_1}(t)\sigma_{z_2}(t)\rangle \approx \langle\sigma_{z_1}(0)\sigma_{z_2}(0)\rangle$, during the desirable QND measurements. As a consequence, one can easily solve the above Eqs. (23a-e) and finally obtain the exact steady-state distribution of the intracavity photon number

$$\frac{\langle \hat{a}^\dagger \hat{a} \rangle_{ss}}{\epsilon^2} = \frac{2}{\kappa} \text{Re} \left\{ \frac{F(\sum_{j,j'} B_j D_{j'} G_j + D_1 D_2) + B_1 B_2 [G_{12}(D_1 + D_2) + \sum_{j,j'} E_j G_{j'}] - \sum_j B_j E_j (D_j + B_j G_j)}{\sum_{j,j'} B_j E_j (D_{j'} F + D_j A) - (B_1 E_1 - B_2 E_2)^2 - A D_1 D_2 F} \right\},$$

$$j, j' = 1, 2, j \neq j'. \quad (24)$$

Here, $A = i\Delta_{dr} - \frac{\kappa}{2}$, $B_j = i\Gamma_j$, $D_j = i\Delta_{dr} - \frac{\kappa}{2} - \gamma_{1,j}$, $E_j = i\Gamma_j + \gamma_{1,j}$, $F = i\Delta_{dr} - \frac{\kappa}{2} - \gamma_{1,j} - \gamma_{1,j'}$, $G_j = \langle \sigma_{z_j}(0) \rangle$, and $G_{12} = \langle \sigma_{z_1}(0) \sigma_{z_2}(0) \rangle$.
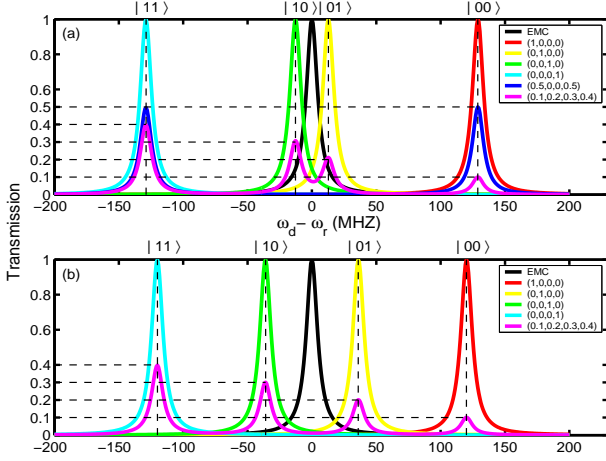

FIG. 3: (Color online) (a). Cavity transmission of the cavity versus the probe detuning $\omega_d - \omega_r$ for certain slected two-qubit states with $|\alpha_0|^2 = 1$, $|\alpha_1|^2 = 1$, $|\alpha_2|^2 = 1$, $|\alpha_3|^2 = 1$, $(|\alpha_0|^2, |\alpha_1|^2, |\alpha_2|^2, |\alpha_3|^2) = (0.5, 0, 0, 0.5)$, and $(|\alpha_0|^2, |\alpha_1|^2, |\alpha_2|^2, |\alpha_3|^2) = (0.1, 0.2, 0.3, 0.4)$, respectively. For comparison, the empty cavity (EMC) transmission is also plotted in black line. Here, The parameters are $(\Gamma_1, \Gamma_2, \kappa, \gamma_{1,1}, \gamma_{1,2}) = 2\pi \times (-11.11, -9.11, 1.7, 0.02, 0.022,)$MHz [16, 20]. In (b) only the parameters Γ_1 and Γ_2 are modified as $\Gamma_1' = 1.05\Gamma_1$ and $\Gamma_2' = 0.85\Gamma_2$. In this case, the relative heights of the peaks are exactly equivalent to the corresponding probabilities of the single logic states superposed in the measured superposition state.

We now investigate the above distributions schematically for various typically selected two-qubit initial states. First, we assume that the two-qubit is initially prepared at only one of the four logic states, i.e., in the generic expression $|\psi\rangle_2 = \alpha_1|00\rangle + \alpha_2|01\rangle + \alpha_3|10\rangle + \alpha_4|11\rangle$ only one of the four probability amplitudes equals 1, e.g., $\alpha_1 = 1$, $\alpha_2 = \alpha_3 = \alpha_4 = 0$. Fig. 3 shows clearly that single peaks reveal the inputs of these four single logic states, and they can also be distinguished by the shifts of the central frequencies of the transmission spectrum. The peaks with frequency shifts: $-\Gamma_1 - \Gamma_2$, $-\Gamma_1 + \Gamma_2$, $\Gamma_1 - \Gamma_2$, and $\Gamma_1 + \Gamma_2$ mark the state $|00\rangle$, $|01\rangle$, $|10\rangle$, and $|11\rangle$, respectively. Thus the pulls of the cavity are strongly dependent of the states of the qubits. For these single logic states the heights of the single peaks are exactly equivalent and of unity value, which is the same as that for the EMC. Next, for the superposition of the four single logic states the situations are quite different. For example, Fig. 3 (a)

also shows that, if the two-qubit is prepared initially as one of the Bell states: $(|\alpha_1|^2, |\alpha_2|^2, |\alpha_3|^2, |\alpha_4|^2) = (0.5, 0, 0, 0.5)$, then the transmitted spectrum of the cavity reveals two peaks; their locations are respectively at the positions for the single states $|00\rangle$ and $|11\rangle$, but have the same relative heights. Moreover, for a more generic superposed state $(|\alpha_1|^2, |\alpha_2|^2, |\alpha_3|^2, |\alpha_4|^2) = (0.1, 0.2, 0.3, 0.4)$ one can see that four peaks are exhibited simultaneously. The central positions of these peaks locate at the corresponding positions of single logic states $|00\rangle$, $|01\rangle$, $|10\rangle$, and $|11\rangle$, respectively. The relative heights of them read 0.1, 0.212, 0.308, and 0.4, respectively. Here, the relative heights of the peaks marking the states $|00\rangle$ and $|11\rangle$ are exactly equivalent to the superposed probabilities $|\alpha_1|^2$ and $|\alpha_4|^2$. However, the relative heights of the peaks marking the states $|01\rangle$ and $|10\rangle$ deviate from the corresponding superposed probabilities $|\alpha_2|^2$ and $|\alpha_3|^2$. This is because these two peaks are not well distinguished due to the contributions from these two logic states' overlap. As a consequence, each peak is higher a little than the expected one, i.e., the superposed probability of the relevant logic state. While, such a situation does not exist for the $|00\rangle$ and $|11\rangle$ peaks (the relative heights of them equal to the expected ones), as they are separated sufficiently far from the others. In Fig. 3 (b) we modify the relevant parameters such as $\Gamma_1' = 1.05\Gamma_1$ and $\Gamma_2' = 0.85\Gamma_2$. Then we find that each peak of the transmission of the cavity is well separated from the others, and thus its relative height is exactly equal to the expectable superposed probability of the corresponding logic state in the measured two-qubit state.

B. High efficiency tomographic reconstruction of a two-qubit state

The two-qubit state tomography is done in the same way as that for the single-qubit state. The only difference is that now there are 15 real parameters to be determined in the 4-dimensional density matrix operator ρ_2, and thus more operations are required to transfer the nondiagonal elements in ρ_2 to the diagonal locations. Generally, the 4-dimensional density matrix for a two-qubit state $|\psi\rangle_2 = \alpha_1|00\rangle + \alpha_2|01\rangle + \alpha_3|10\rangle + \alpha_4|11\rangle$ in a complete basis $\{|1\rangle_2 = |00\rangle, |2\rangle_2 = |01\rangle, |3\rangle_2 = |10\rangle, |4\rangle_2 = |11\rangle\}$ can be represented as

$$\rho_2 = \begin{pmatrix} \rho_{11} & \rho_{12} & \rho_{13} & \rho_{14} \\ \rho_{21} & \rho_{22} & \rho_{23} & \rho_{24} \\ \rho_{31} & \rho_{32} & \rho_{33} & \rho_{34} \\ \rho_{41} & \rho_{42} & \rho_{43} & \rho_{44} \end{pmatrix}, \quad (25)$$

which can also be rewritten as $\rho_2 = \bar{\rho}_2/4$ with [5]

$$\bar{\rho}_2 = \sum_{m,n=0,x,y,z} r_{mn}\sigma_{m_1} \otimes \sigma_{n_2}$$

$$= \begin{pmatrix} r_{00} + r_{0z} + r_{z0} + r_{zz} & r_{0x} + r_{zx} - ir_{0y} - ir_{zy} & r_{x0} + r_{xz} - ir_{y0} - ir_{yz} & r_{xx} - r_{yy} - ir_{xy} - ir_{yx} \\ r_{0x} + r_{zx} + ir_{0y} + ir_{zy} & r_{00} - r_{0z} + r_{z0} - r_{zz} & r_{xx} + r_{yy} + ir_{xy} - ir_{yx} & r_{x0} - r_{xz} - ir_{y0} + ir_{yz} \\ r_{x0} + r_{xz} + ir_{y0} + ir_{yz} & r_{xx} + r_{yy} - ir_{xy} + ir_{yx} & r_{00} + r_{0z} - r_{z0} - r_{zz} & r_{0x} - r_{zx} - ir_{0y} + ir_{zy} \\ r_{xx} - r_{yy} + ir_{xy} + ir_{yx} & r_{x0} - r_{xz} + ir_{y0} - ir_{yz} & r_{0x} - r_{zx} + ir_{0y} + ir_{zy} & r_{00} - r_{0z} - r_{z0} + r_{zz} \end{pmatrix}.$$

(26)

Here, $\sigma_{m=x,y,z}$ are the Pauli operators and σ_0 identity matrix, and what we want to determine is sixteen real parameters r_{mn}. Note that the first and second subscripts of the matrix elements ρ_{ij} (i, j=1, 2, 3, 4) in Eq. (25) and r_{mn} in Eq. (26) is labeled for the first and second qubits, respectively.

As in the above discussion, performing the QND measurements on the two-qubit state ρ_2 can directly determine all the four diagonal elements: ρ_{11}, ρ_{22}, ρ_{33} and ρ_{44}, respectively, by the measured results $|\alpha_1|^2$, $|\alpha_2|^2$, $|\alpha_3|^2$ and $|\alpha_4|^2$. As a consequence, the parameters r_{00}, r_{0z}, r_{z0} and r_{zz} can be determined by

$$\begin{aligned} r_{00} &= |\alpha_1|^2 + |\alpha_2|^2 + |\alpha_3|^2 + |\alpha_4|^2 = 1, \\ r_{0z} &= |\alpha_1|^2 - |\alpha_2|^2 + |\alpha_3|^2 - |\alpha_4|^2, \\ r_{z0} &= |\alpha_1|^2 + |\alpha_2|^2 - |\alpha_3|^2 - |\alpha_4|^2, \\ r_{zz} &= |\alpha_1|^2 - |\alpha_2|^2 - |\alpha_3|^2 + |\alpha_4|^2. \end{aligned}$$

(27)

To determine the other 12 parameters, we need to perform certain unitary operations to transfer them to the diagonal locations for other QND measurements.

It is well-known that, arbitrary two-qubit operation assisted by arbitrary rotations of the single qubits generate an universal set of quantum gates. So the key to implement the above required operations for tomographies is to realize a two-qubit gate. Again, for the experimental circuit QED system with two superconducting charge qubits, such a gate could be implemented by using the so-called FLICFORQ protocol [24]. In fact, if the cavity is driven by two external fields satisfying the sideband matching condition: $\omega_{d_2} - \omega_{d_1} = \Omega_1 + \Omega_2$, then an effective Hamiltonian

$$\tilde{H}_{\mathrm{FF}} = \omega_r \hat{a}^\dagger \hat{a} + \frac{g_1 g_2 (\Delta_1' + \Delta_2')}{16\Delta_1'\Delta_2'}(\sigma_{y_1} \otimes \sigma_{y_2} + \sigma_{z_1} \otimes \sigma_{z_2}),$$

(28)

can be induced in a quadruply rotating framework. Here, $\Delta_j' = \omega_j + 2\Omega_{jj'}^2/\Delta_{jd_{j'}} - \omega_r$ with $\Omega_{jj'} = 2g_j\epsilon_{j'}/(\omega_{d_{j'}} - \omega_r)$, and $\Delta_{jd_{j'}} = \omega_j - \omega_{d_{j'}}$, $j, j' = 1, 2, j \neq j'$. Obviously, the evolution under the above Hamiltonian with the duration, e.g., around ~ 100ps, for the experimental parameters [24], can produce a two-qubit operation:

$$U_{\mathrm{FF}} = \exp[i\pi(\sigma_{y_1} \otimes \sigma_{y_2} + \sigma_{z_1} \otimes \sigma_{z_2})/4].$$

(29)

On the other hand, the typical single-qubit gates, e.g., U_{x_j}, U_{y_j}, and U_{z_j} (j=1, 2) can be relatively easy to produce

using the similar approaches presented in Sec. III. With such a two-qubit operation and these single-qubit gates, we show in Table I how to perform the desirable unitary operations for transferring the non-diagonal elements to the diagonal locations. For example, by performing a selected operational sequence $W = U_{\mathrm{FF}}U_{x_1}$ on the original density matrix ρ_2, we have a new density matrix $\rho_2' = W\rho_2 W^\dagger$, and the new diagonal elements are

$$\begin{aligned} \rho_{11}' &= \frac{1}{4}(r_{00} + r_{xy} - r_{yz} + r_{zx}), \\ \rho_{22}' &= \frac{1}{4}(r_{00} + r_{xy} + r_{yz} - r_{zx}), \\ \rho_{33}' &= \frac{1}{4}(r_{00} - r_{xy} + r_{yz} + r_{zx}), \\ \rho_{44}' &= \frac{1}{4}(r_{00} - r_{xy} - r_{yz} - r_{zx}). \end{aligned}$$

(30)

Then, by the QND measurements the values of $|\alpha_1'|^2$, $|\alpha_2'|^2$, $|\alpha_3'|^2$, and $|\alpha_4'|^2$ are given directly. As a consequence, the desirable parameters r_{00}, r_{xy}, r_{yz} and r_{zx} can be obtained by the relations:

$$\begin{aligned} r_{00} &= |\alpha_1'|^2 + |\alpha_2'|^2 + |\alpha_3'|^2 + |\alpha_4'|^2 = 1, \\ r_{xy} &= |\alpha_1'|^2 + |\alpha_2'|^2 - |\alpha_3'|^2 - |\alpha_4'|^2, \\ r_{yz} &= -|\alpha_1'|^2 + |\alpha_2'|^2 + |\alpha_3'|^2 - |\alpha_4'|^2, \\ r_{zx} &= |\alpha_1'|^2 - |\alpha_2'|^2 + |\alpha_3'|^2 - |\alpha_4'|^2. \end{aligned}$$

(31)

Similarly, other non-diagonal elements can also be determined. Clearly, here only six kinds of QND measurements are sufficient to tomographically reconstruct a two-qubit state. This is obviously simpler than the previous tomographies based on the usual DP measurements, wherein 15 kinds of measurements are probably required [5, 20]. Thus, the present tomographies is essentially high efficient.

After performing all the QND measurements listed in the table, a two-qubit state can be completely reconstructed. For example, a two-qubit state ρ_2 having the following representation:

$$\rho_2 = \begin{pmatrix} r_{00} & r_{0x} & r_{0y} & r_{0z} \\ r_{x0} & r_{xx} & r_{xy} & r_{xz} \\ r_{y0} & r_{yx} & r_{yy} & r_{yz} \\ r_{z0} & r_{zx} & r_{zy} & r_{zz} \end{pmatrix} = \begin{pmatrix} 1 & 0 & 0 & -\frac{1}{5} \\ 0 & \frac{1}{4} & 0 & \frac{3}{5} \\ 0 & 0 & -\frac{1}{4} & 0 \\ -\frac{2}{5} & \frac{1}{8} & 0 & 0 \end{pmatrix},$$

(32)

which can be effectively reconstructed by these parameters

$$\rho_2 = \begin{pmatrix} \rho_{11} & \rho_{12} & \rho_{13} & \rho_{14} \\ \rho_{21} & \rho_{22} & \rho_{23} & \rho_{24} \\ \rho_{31} & \rho_{32} & \rho_{33} & \rho_{34} \\ \rho_{41} & \rho_{42} & \rho_{43} & \rho_{44} \end{pmatrix} = \begin{pmatrix} 0.1 & 0.0313 - 0.0313i & 0.15 - 0.15i & -0.125i \\ 0.0313 + 0.0313i & 0.2 & 0.125 & -0.15 + 0.15i \\ 0.15 + 0.15i & 0.125 & 0.3 & -0.0313 + 0.0313i \\ 0.125i & -0.15 - 0.15i & -0.0313 + 0.0313i & 0.4 \end{pmatrix}, \quad (33)$$

TABLE I: The operational combinations before the QND measurements to determine the parameters for tomographically reconstructing a two-qubit state. The subscript "1(2)" of U is labeled for the operation of qubit 1(2).

quantum operation W	determined parameters
no	$r_{00}, r_{zz}, r_{0z}, r_{z0}$
$U_{\mathrm{FF}}U_{x_1}$	$r_{00}, r_{xy}, r_{yz}, r_{zx}$
$U_{\mathrm{FF}}U_{y_1}$	$r_{00}, r_{yx}, r_{zy}, r_{xz}$
$U_{\mathrm{FF}}U_{z_1}$	$r_{00}, r_{xx}, r_{yy}, r_{zz}$
$U_{y_1}U_{z_1}U_{\mathrm{FF}}$	$r_{00}, r_{0x}, r_{y0}, r_{yx}$
$U_{y_2}U_{z_2}U_{\mathrm{FF}}$	$r_{00}, r_{x0}, r_{0y}, r_{xy}$

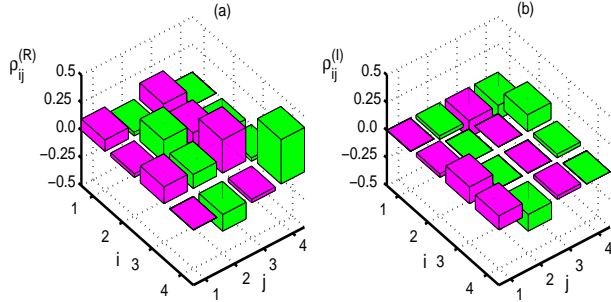determined by six kinds of QND measurements. The simulated reconstructions are graphically shown in Fig. 4, where $\rho_i^{(}$ n- st $\rangle$, |3

FIG. 4: (Color online) Schematic representations of the density matrix ρ_2 for a two-qubit state. The real $\rho_{ij}^{(R)}$ and imaginary $\rho_{ij}^{(I)}$ parts $(i, j = 1, 2, 3, 4)$ of the density matrix elements in the complete bases are plotted in (a) and (b), respectively.

V. DISCUSSIONS AND CONCLUSIONS

Generally, the quantum state tomographic constructions demonstrated above can be extended for N (with $N > 2$) qubits in a straightforward manner. This is because that the proposed QND measurements can be directly applied to determine all the diagonal elements of the arbitrary N-qubit state; the individual superposed logic states can be inferred from the relevant positions of the measured peaks, and the probabilities of the corresponding computational bases superposed in the measured state could be extracted from the relative heights of the peaks (when they separate sufficiently from the others). Moreover, all the required operations for the tomographic reconstructions can be implemented from the universal set of the logic gates demonstrated.

In summary, we have proposed a scheme to perform the quantum state tomographies by QND measurements. Differing from the usual tomographies based on the DP measurements, here the QND measurements are utilized. Since all the diagonal elements of the density matrix of an unknown quantum state can be simultaneously determined by a single kind of QND measurements, the efficiency of the present tomographic reconstruction is definitely better for more qubits. Specifically, our proposal is demonstrated with the current circuit QED setup with a few charge qubits, and could be generalized to other systems, in principle.

[1] M. G. A. Paris and J. Řeháček, *Quantum State Estimation*, Lect. Not. Phys. Vol. 649 (Springer, Berlin, 2004)

[2] A. G. White, D. F. V. James, P. H. Eberhard, and P. G. Kwiat, Phys. Rev. Lett. **83**, 3103 (1999)

[3] N. K. Langford, R. B. Dalton, M. D. Harvey, J. L. O'Brien, G. J. Pryde, A. Gilchrist, S. D. Bartlett, and A. G. White, Phys. Rev. Lett. **93**, 053601 (2004)

[4] H. Häffner, W. Hänsel, C. F. Roos, J. Benhelm, D. C. al kar, M. Chwalla, T. Körber, U. D. Rapol, M. Riebe, P. O. Schmidt,

C. Becher, O. Gühne, W. Dür, and R. Blatt, Nature **438**, 643 (2005)

[5] Yu-xi Liu, L. F. Wei, and F. Nori, Europhys. Lett. **67**, 874 (2004); Yu-xi Liu, L. F. Wei, and F. Nori, Phys. Rev. B **72**, 014547 (2005)

[6] V. B. Braginsky and F. Ya. Khalili, Rev. Mod. Phys. **68**, 1 (1996)

[7] S. F. Pereira, Z. Y. Ou, and H. J. Kimble, Phys. Rev. Lett. **72**, 214 (1994)

[8] K. Bencheikh, J. A. Levenson, Ph. Grangier, and O. Lopez,

Phys. Rev. Lett. **75**, 3422 (1995)

[9] P. Grangier, J. A. Levenson and J. P. Poizat Nature (London) **396**, 537(1998)

[10] J. A. Levenson, I. Abram, T. Rivera, P. Fayolle, J. C. Garreau, and P. Grangier, Phys. Rev. Lett. **70**, 267 (1993)

[11] H. M. Wiseman, Phys. Rev. A **51**, 2459 (1995)

[12] G. Nogues, A. Rauschenbeutel, S. Osnaghi, M. Brune, J. M. Raimond, and S. Haroche, Nature (London) **400**, 239 (1999)

[13] Q. A. Turchette, C. J. Hood, W. Lange, H. Mabuchi, and H. J. Kimble, Phys. Rev. Lett. **75**, 4710 (1995)

[14] A. Blais, R. S. Huang, A. Wallraff, S. M. Girvin, and R. J. Schoelkopf, Phys. Rev. A **69**, 062320(2004)

[15] A. Wallraff, D. I. Schuster, A. Blais, L. Frunzio, R. S. Huang, J. Majer, S. Kumar, S. M. Girvin, and R. J. Schoelkopf, Nature (London) **431**, 162(2004)

[16] A. Wallraff, D. I. Schuster, A. Blais, L. Frunzio, J. Majer, M. H. Devoret, S. M. Girvin, and R. J. Schoelkopf, Phys. Rev. Lett. **95**, 060501(2005)

[17] L. F. Wei, Yu-xi Liu, C. P. Sun, and Franco Nori, Phys. Rev. Lett. **97**, 237201 (2006).

[18] J. Gambetta, A. Blais, M. Boissonneault, A. A. Houck, D. I. Schuster, and S. M. Girvin, Phys. Rev. A **77**, 012112 (2008)

[19] R. Bianchetti, S. Filipp, M. Baur, J. M. Fink, M. Göppl, P. J. Leek, L. Steffen, A. Blais, and A. Wallraff, Phys. Rev. A **80**, 043840(2009)

[20] S. Filipp, P. Maurer, P. J. Leek, M. Baur, R. Bianchetti, J. M. Fink, M. Göppl, L. Steffen, J. M. Gambetta, A. Blais, and A. Wallraff, Phys. Rev. Lett. **102**, 200402 (2009)

[21] L. F. Wei, J. S. Huang, X. L. Feng, Z. D. Wang and C. H. Oh, arXiv: 1005. 2470

[22] D. F. Walls and G. J. Milburn, *Quantum Optics* (Spinger-Verlag, Berlin, 1994)

[23] Y. Makhlin, G. Schön, and A. Shnirman, Rev. Mod. Phys. **73**, 357 (2001)

[24] A. Blais, J. Gambetta, A. Wallraff, D. I. Schuster, S. M. Girvin, M. H. Devoret, and R. J. Schoelkopf, Phys. Rev. A **75**, 032329 (2007)